Ultra-High Dose Rate Helium Ion Beams: First In Vivo Evidence for Neuroprotective FLASH Effect

Ivana Dokic[1-5], Thomas Tessonnier[1,5], Sarah Meister[1-5], Mahmoud Moustafa[1-6], Federica Ciamarone[1-5], Damir Krunic[7], Thomas Haberer[5], Jürgen Debus[1-5], Andrea Mairani[1,5,8] and Amir Abdollahi[1-5]

[1]*Clinical Cooperation Unit Translational Radiation Oncology, National Center for Tumor Diseases (NCT), Heidelberg University Hospital (UKHD) and German Cancer Research Center (DKFZ), Im Neuenheimer Feld 460, Heidelberg, Germany*
[2]*Division of Molecular and Translational Radiation Oncology, Department of Radiation Oncology, Heidelberg Faculty of Medicine (MFHD) and Heidelberg University Hospital (UKHD), Heidelberg Ion-Beam Therapy Center (HIT), Im Neuenheimer Feld 450, 69120 Heidelberg, Germany*
[3]*German Cancer Consortium (DKTK) Core-Center Heidelberg, German Cancer Research Center (DKFZ), Im Neuenheimer Feld 280, Heidelberg, Germany*
[4]*Heidelberg Institute of Radiation Oncology (HIRO), National Center for Radiation Oncology (NCRO), Heidelberg University and German Cancer Research Center (DKFZ), Im Neuenheimer Feld 222, Heidelberg, Germany*
[5]*Heidelberg Ion-Beam Therapy Center (HIT), Im Neuenheimer Feld 450, Heidelberg, Germany*
[6] *Department of Clinical Pathology, Suez Canal University, Ismailia, Egypt*
[7] *Light Microscopy Facility, German Cancer Research Center (DKFZ), 69120 Heidelberg, Germany*
[8]*National Center for Oncological Hadrontherapy (CNAO), Str. Campeggi 53, Pavia, Italy.*

Corresponding Author(s):
Ivana Dokic PhD
National Center for Tumor Diseases (NCT)
In Neuenheimer Feld 460
Heidelberg, 69120, Germany
+49 (0)6221-56-35275
i.dokic@dkfz.de

Running Title: Helium ions FLASH therapy in vivo

Source of Funding: This work was supported by intramural funds from National Center for Tumor diseases (NCT-PRO and Biodose programs) and German Cancer Consortium (DKTK), and in part by National Institutes of Health (NIH-1P01CA257904-01A1) and the collaborative research center of the German research foundation (DFG, Unite, SFB-1389, Project number 404521405). The funders had no role in study design, data collection and analysis, decision to publish or preparation of the manuscript.

Conflicts of Interest: JD reports grants from CRI – The Clinical Research Institue GmbH grants from View Ray Inc., grants from Accuray International Sarl, grants from Accuray Incorposrated, grants from RaySearch Laboratories AB, grants from Vision RT limited, grants from Merck Serono GmbH, grants from Astellas Pharma GmbH, grants from Astra Zeneca GmbH, grants from Siemens Healthcare GmbH, grants from Merck KGaA Accounts Payable, grants from Solution Akademie GmbH, grants from Ergomed PLC Surrey Research Park, grants from Siemens Healthcare GmbH, grants from Quintiles GmbH, grants from Pharmaceutecal Research Associates GmbH, grants from Boehringer Ingelheim Pharma GmbH Co, grants from PTW-Freiburg Dr. Pychlau GmbH. AA report grants and other from Merck and EMD, grants and other from Fibrogen, other from BMS, other from BioMedX, other from Roche, outside the submitted work.

Statistical Analyses were performed by I.D. (i.dokic@dkfz.de; +49 (0)6221-56-35275)

Data Sharing: Research data are stored in an institutional repository and will be shared upon request to the authors.

Acknowledgments: The authors thank Dr. Stephan Brons and the entire HIT accelerator team for establishing and providing the FLASH ion beam. The authors thank Ms. Lena Vogelbacher for excellent technical support.

Abstract

Purpose: To investigate ultra-high-dose rate helium ion irradiation and its potential FLASH sparing effect with the endpoint acute brain injury in preclinical in vivo settings.

Material and methods: Raster-scanned helium ion beams were administered to explore and compare the impact of dose rate variations between standard dose rate (SDR at 0.2 Gy/s) and FLASH (at 141 Gy/s) radiotherapy (RT). Irradiation-induced brain injury was investigated in healthy C57BL/6 mice via DNA damage response kinetic studies using nuclear γH2AX as a surrogate for double-strand breaks (DSB). The integrity of the neurovascular and immune compartments was assessed via CD31+ microvascular density and microglia/macrophages activation. Iba1+ ramified and CD68+ phagocytic microglia/macrophages were quantified, together with the expression of inducible nitric oxide synthetase (iNOS).

Results: Helium FLASH RT significantly prevented acute brain tissue injury compared with SDR. This was demonstrated by reduced levels of DSB and structural preservation of the neurovascular endothelium after FLASH RT. Moreover, FLASH RT exhibited reduced activation of neuroinflammatory signals compared with SDR, as detected by quantification of CD68+ iNOS+ microglia/macrophages.

Conclusion: To our knowledge, this is the first report on the FLASH-sparing neuroprotective effect of raster scanning helium ion radiotherapy in vivo.

Key words: FLASH radiotherapy, helium ion beams, neuro-inflammation, DDR, neurovascular interface, neuroglia, microenvironment, acute brain injury

Introduction

Helium ion radiotherapy provides exceptional precision in targeting tumors due to the Bragg peak phenomenon and reduced lateral scattering. This modality has gained prominence in the radiation oncology community because of its potential to minimize damage to healthy surrounding tissues despite conformal coverage of the tumor volume [1]. Moreover, helium ions are characterized by a higher linear energy transfer (LET) compared to e.g. protons. This results in more effective DNA damage, which may lead to improved tumor control and enhance therapeutic efficacy. Helium ions are particularly noteworthy for their significantly reduced lateral scattering, which is approximately 50% smaller than that observed with protons [2]. Helium ions are being actively explored as a potential alternative to proton therapy, with in silico indications suggesting potentially better outcomes under certain clinical scenarios [3]. The risk of healthy tissue damage during radiotherapy can be reduced using helium ions [4], which can be further optimized using ultra high dose rate delivery (FLASH). Healthy tissue sparing using ultra high-dose rate deliveries has been predominantly known for electrons and, more recently, proton beams [5-8]. Considering helium ions, two studies have shown that ultra-high dose rate helium beams have significant potential for FLASH sparing effect in vitro [9] and in vivo in a zebrafish model [10]. The best of our knowledge, this is the first study describing FLASH effect with raster scanning helium ions in a preclinical mouse model. In the current study, we investigated the effects of FLASH irradiation,

focusing on the brain endothelium and microglia/macrophages. These two components are encompassed in neurovascular unit (NVU) [11] and play a critical role in maintaining brain homeostasis [12]. Endothelial cells within the blood brain barrier (BBB) and NVU express CD31, which can serve as an indicator of endothelial BBB integrity [13]. Reduced CD31 signal may imply BBB/endothelium compromise [14], which is potentially linked to irradiation injury with microglia activation [15]. The activation of microglia, which are the primary immune cells in the brain [16], plays a crucial role in the brain's response to radiation [15]. Microglia can reside in resting state or activated state. Whereas resting state is characterized by ramified cellular morphology, activation of microglia is followed by a change to ameboid morphology [17, 18]. It is well-established that irradiation induced microglial activation can lead to neural tissue toxicity [19], trigger a potentially damaging neuroinflammatory response [20], and contribute to cognitive impairment [21]. Among various markers of microglial activation, a general phagocytic marker of activated microglia-CD68 [22] has been found to be upregulated in response to helium ion irradiation induced stress [23]. Another marker of microglial response to stress stimuli is increased expression of inducible nitric oxide synthase (iNOS) [24, 25]. Nitric oxide (NO) is a regulatory molecule that play a role in regulating brain homeostasis under physiological conditions [26]. The objective of our study was to explore the potential helium ion FLASH effect in brain tissue using these markers as a proxy for brain damage.

Methods and Materials

Planning and irradiation

Treatment plan was consisting of 16 spots, with a 4 mm spot spacing at isocenter, resulting in a 12x12 mm² field. The irradiation setup was located near the beam exit and included a 2D ridge filter (to create a 2 cm spread out Bragg peak (SOBP)) and PMMA absorber as previously described [9]. The plan was optimized to deliver 10 Gy in the center of each brain (~3.9 mm below the skin) for a maximum dept of ~6 mm, for both standard dose rate SDR and FLASH irradiations with 145.74 MeV/u helium beams (full width at half maximum (FWHM) in air at isocenter 6.8 mm). The total number of particles used was 2.82E9. For SDR irradiations, the delivery of the mono-energetic layer was divided into 10 spills to achieve an average dose rate closer to clinical scenarios (~0.2 Gy/s). A collimator (material: PMMA; thickness 1cm, aperture: 6 x 6 mm²) was placed on top of the mouse heads, with a 2.5 cm air gap after a 112 mm PMMA range shifter. The collimator helped to enhance target precision for small volumes resulting in an iso-line above 90% of the planned dose of 5 x 5 mm^2. For in silico verification and physical distribution quantification, a detailed geometry of the in vivo experimental set-up was incorporated into the in-house FLUKA Monte Carlo (MC) simulation system, including specifications of the HIT beam-line. Simulations were performed for dose and dose-averaged linear energy transfer (LET_D) prediction. For both delivery cases, measurements with ionization chamber (PinPoint chamber 31015, PTW) following TRS398 were performed to verify the dose at the desired position, with and without collimator. Additional verifications were performed with EBT gafchromic films.
As summarized in Table 1, for the 10 spills separated by about 5.3 seconds from each other (inter-spill time), the accelerating system delivered 1 Gy to each mouse in 380 ms (spill time), for a total irradiation time of around 48 seconds (delivery time). For FLASH irradiations, the delivery of the 10 Gy was made in one spill of ~70 ms achieving ~141 Gy/s dose rate. Raster-scanning of the 16-spot plan was performed at ~4.5 ms/spot.

Animal model

Six-week-old female C57BL/6 mice (Janvier Labs) were used in this study. Mice were anesthetized with isoflurane for irradiation and fixed in a custom-made holder during irradiation. A collimator was placed over the head of each mouse, sparing an area of 6 x 6 mm^2 above the right hemisphere as the irradiation field. Animal work was carried out in accordance with the rules approved by the local and governmental animal care committee established by the German government (Regierungspraesidium, Karlsruhe).

Tissue preparation and immunofluorescence

Tissue was prepared and stained as described [27]. Briefly, mice were anesthetized with 120 mg/kg ketamine (Ketaset, Zoetis) and 20 mg/kg xylazin (Rompun, Bayer) and transcardially perfused with ice-cold PBS (Gibco) followed by ice-cold 4% PFA (Carl Roth) in PBS. The mice were decapitated and brains were fixed in 4% paraformaldehyde and cryoprotected with 30% sucrose (Roth) in PBS until they sank. Brains were placed in Tissue-Tek Cryomolds (Sakura Finetek) and embedded in Tissue-Tek O.C.T. Compound (Sakura Finetek) before slow freezing in isopentane (2-Methylbutane, Honeywell; pre-cooled in liquid nitrogen) and subsequent storage at -80°C. Brains were sagittally sectioned (thickness 8–10 µm) on a cryotome (CryoStar NX70; Thermo Scientific).

Sections were thawed at room temperature, washed, and blocked using blocking buffer containing 2.5% goat serum, 1% bovine serum albumin (BSA), and 0.1% Triton X in phosphate-buffered saline (phosphate-buffered saline (PBS)) and ReadyProbesTM Mouse-on-Mouse IgG Blocking Solution (Invitrogen, Carlsbad, CA, USA) according to the manufacturer's instructions. CD31 (Abcam, 1:50) antibody was used for endothelial cell and blood vessel assessment. Iba1 (1:500) and CD68 antibody (1:100, Bioss antibodies) were used for microglia/macrophage identification. iNOS was used as a marker of microglia activation (Abcam, 1:100). Slides were washed and signals were detected using Alexa Fluor 647 (γH2AX, Iba1, CD68), Alexa Fluor 555 (CD31) or Alexa Fluor 488 (iNOS) (Invitrogen) as secondary antibodies (1:400). Specificity of staining was confirmed using negative controls where only secondary antibody was applied on the samples. DAPI (1:1000, Sigma Aldrich) dye was used to stain nuclei.

Microscopy and image analysis

Zeiss Axio Scan.Z1 microscope equipped with a Colibri 5/7 with 385 nm, 567 nm, and 630 nm LEDs, 20x 0.8 Plan-Apo objective and Orca Flash 4.0 V2 sCMOS camera was used for imaging. The images were then analyzed using the high throughput software ScanR Analysis (v3.2) and

ImageJ. For γH2AX, a nuclei detection based on DAPI intensity thresholding was performed followed by a sub-object routine which detected nuclear γH2AX signal above a defined fixed threshold based on the control (non-irradiated) samples. The resulting nuclei which were positive for DAPI and γH2AX were scored. For γH2AX nuclear signal total intensity analysis, total intensities within control samples were averaged and normalized to 1, and total intensity signals from the treated cells were normalized to the averaged control signal. The change in γH2AX total

intensity signal was then expressed as a fold change in comparison to the control. For CD31 detection a thresholding and edge detection method was utilized to detect the CD31 positive blood vessels. $CD31^+$ microvascular density was calculated as the proportion of $CD31^+$ signal area over the total measurement ROI area and expressed as a percentage.
To measure and quantify the percentage of Iba1, CD68 and γH2AX positive cells, in-house developed macros for ImageJ were used. In short, images of DAPI were background subtracted using Rolling Ball algorithm, blurred with Gaussian blur, segmented with Find Maxima tool and thresholded. The output of Find Maxima was Single Points (centers of DAPI stained nuclei). The images of stained area were processed with Rolling Ball Background Subtraction, Gaussian Blur and the selection was created above threshold. All single points (centers of DAPI) within the selected stained area were counted and compared to the total cell count. Number of positive stained cells was normalized to the total number of nuclei. For all images, analyses were performed in irradiated cortical brain area in order to keep structural consistency of the investigated brain region among the samples. Each tissue was analyzed using 12-15 ROIs (each ROI equaled 1000x1000 pixels). Five brains per group were analyzed, except for γH2AX analysis, where three brains per group and per time point were analyzed.

Statistical analysis

Data presentation and statistics were done in GraphPad Prism software. One-way analysis of variance (ANOVA) with Tukey's multiple comparisons test was used to compare the treatment outcomes.

Results

Irradiation parameters and settings

Helium ion beams at SDR and FLASH dose rates were delivered as reported in Table 1. For both SDR and FLASH irradiations, plans were created to deliver 10 Gy for each ion in the center of each mice brain (appx 3.9 mm after the skin) for a maximum depth of ~6 mm. 16 spots mono-energetic layer was created (Fig. 1a), to cover the right hemisphere of the mouse brain. Profiles of dose and LET_D as function of depth within the mice brain and lateral distribution are shown in Fig.1 b and c. Collimation of about 5 x $5mm^2$ was predicted by Monte Carlo simulation and displayed on gafchromic dosimetric film for both FLASH and SDR (Fig. 1d). LET_D range between proximal and distal R_{80} (range at which dose is 80% of the maximum SOBP dose) were from 20 keV μm^{-1} to 40 keV μm^{-1}. For both SDR and FLASH, measurements with an ionization chamber (PinPoint chamber, PTW) were performed to verify the dose at the desired position (Table 1). In order to irradiate the right hemisphere of the mouse brains (Fig. 1e), animals were positioned in holders as previously detailed in [27].

	Dose (Gy)	Delivery time (s)	Interspill Time (s)	Spill time (s)	Delivery mean dose rate (Gy/s)	Interspill mean dose rate (Gy/s)	Instant spill dose rate (Gy/s)
SDR	9.9	48	5.3	0.38	0.2	1.9	26.1
FLASH	9.9	0.07	-	0.07	141.4	-	141.4

Table 1. Irradiation delivery mean parameters

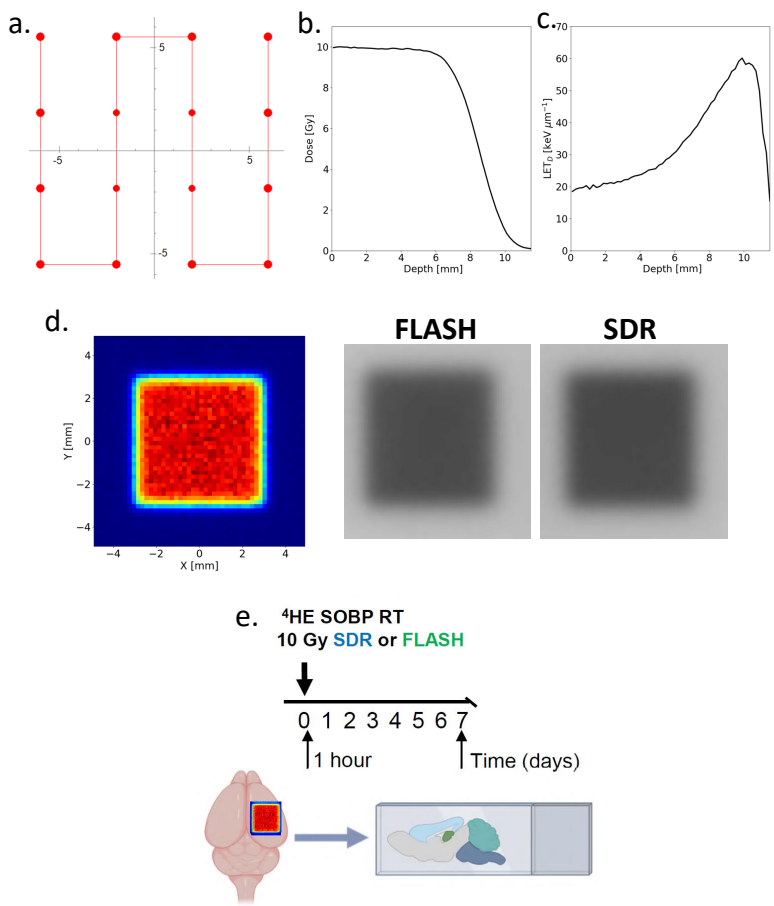

Figure 1. Irradiation setup for the mice irradiation **a.** 16 spots mono-energetic layer was created to cover right hemisphere of mouse. **b.** Monte Carlo simulated depth dose distributions of the 10 Gy SOBP. **c.** Monte Carlo simulated depth dose-avereged LET distributions of the 10 Gy SOBP. **d.** Lateral profile predicted with Monte Carlo and measured with EBT3 for both SDR and FLASH. **e.** Experimental time axis:

mouse brains were isolated and 1 hour or 7 days post-RT and further processed for IHC (created with BioRender.com).

FLASH RT spares brain tissue from DNA damage

To investigate DNA damage in brain tissue, after SDR vs. FLASH helium radiotherapy, we used γH2AX as a double-strand DNA break (DSB) marker. The image analysis indicated significantly reduced intensity of γH2AX nuclear signal after FLASH irradiation, at both early (1h-post RT; p= 0.0083; Fig. 2a) and late (7 days post-RT, p= 0.0001; Fig. 2b) time points. Moreover, the fraction of γH2AX positive nuclei was significantly lower in FLASH-irradiated samples than in SDR-irradiated samples (p= 0.0001), which could indicate for differential double-strand breaks damage formation and/or repair in FLASH vs. SDR RT (Figure 2).

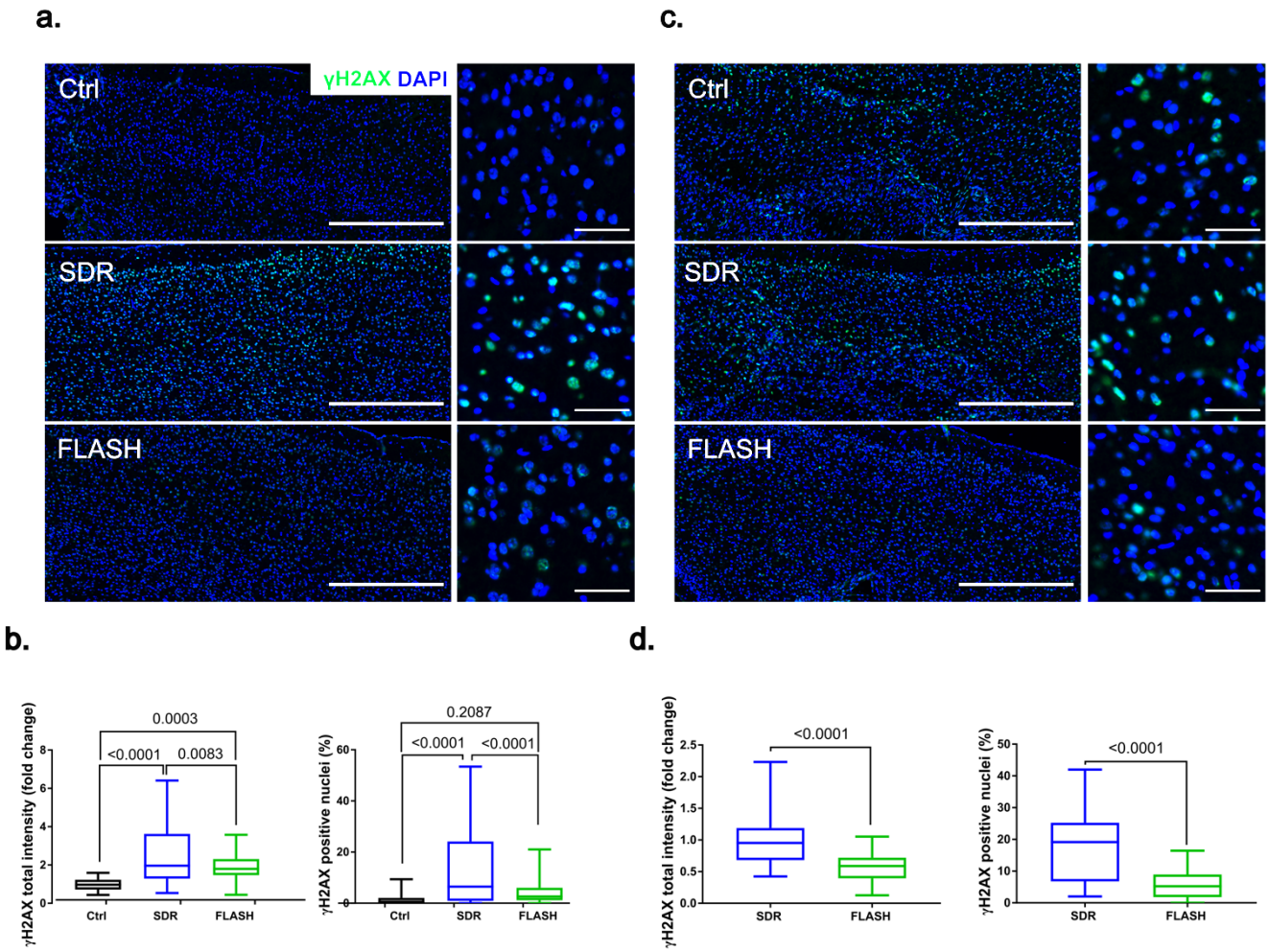

Figure 2. FLASH RT results in lower pS139 H2AX foci (γH2AX) signal in healthy C57BL/6 mouse brain sections. **a.** Representative images and **b.** quantification of γH2AX total intensity (shown as a fold change normalized to the non-irradiated control) and percentage of γH2AX positive nuclei at 1h post-irradiation (n_{Ctrl}=3, n_{SDR}= 3, n_{FLASH}= 3 brains). **c.** Representative images and **d.** quantification γH2AX total intensity

and percentage of γH2AX positive nuclei at 1 7 days n_{Ctrl}=3, n_{SDR}= 3, n_{FLASH}= 3, brains) post-RT. Arrows point to the γH2AX positive nuclei. Non-irradiated samples were used as controls. Data are presented as box and whiskers plots (min, max; horizontal line indicates median). Groups were compared using ANOVA Tukey's post-hoc test. (overview scale bar: 500 µm; zoom scale bar: 50 µm; magnification 20x).

FLASH beams preserve brain microvascular architecture

Structural changes of the $CD31^+$ endothelium were examined to assess the integrity of brain tissue after irradiation. As shown in Fig. 3a, the CD31 signal of the brain microvascular endothelium is more evident for control samples, than in irradiated samples (7 days post-RT). Quantification of $CD31^+$ structures indicated significant decrease in CD31 microvascular density (MVD) after radiotherapy (p= 0.0001, Fig 3b). However, the radiation-induced change in MVD was dose rate-dependent. Brains irradiated with FLASH beams exhibit higher $CD31^+$ MVD in comparison to SDR irradiated tissues (p= 0.018, Fig. 3b).

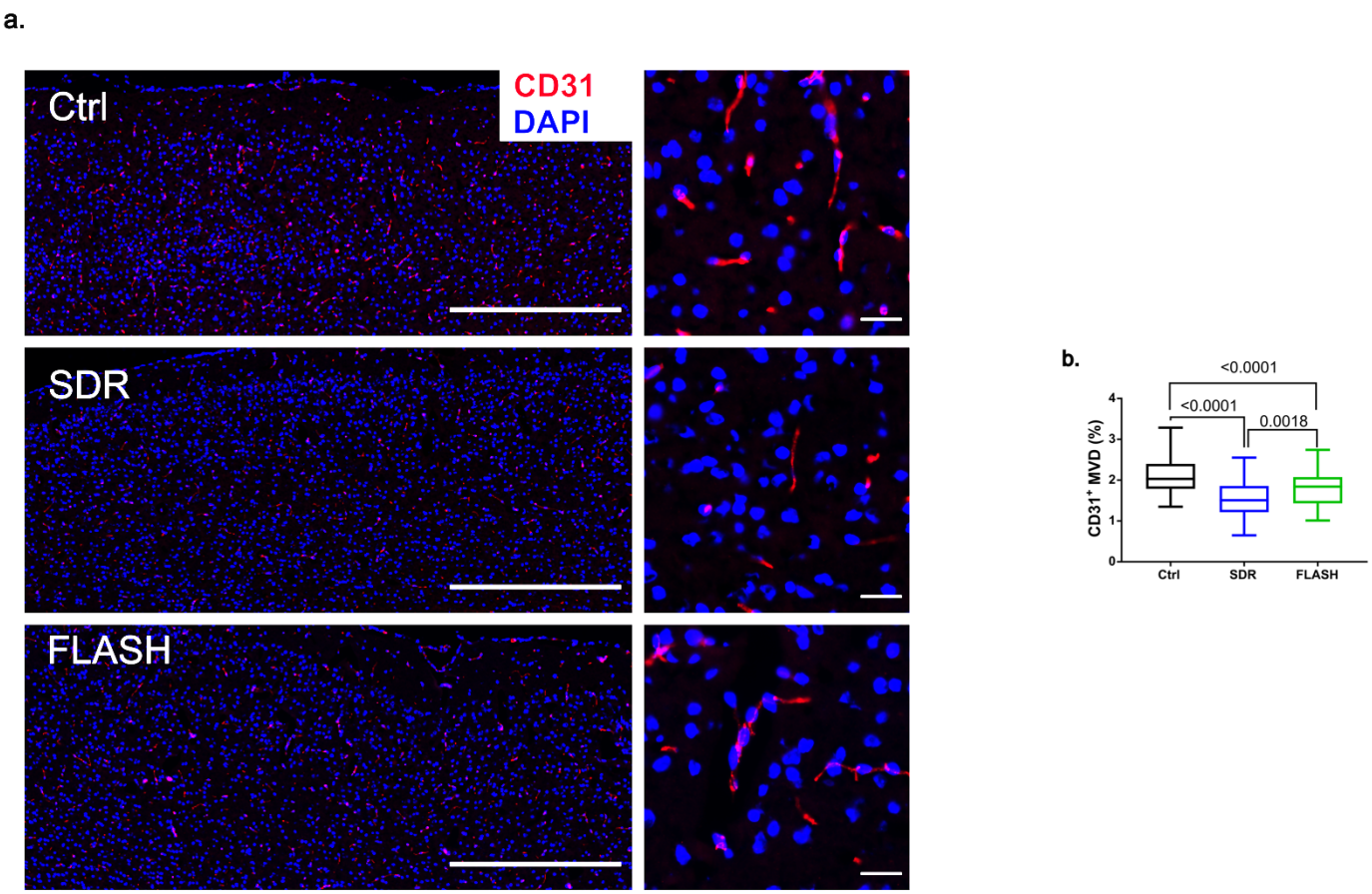

Figure 3. FLASH beams spare brain microvascular architecture. **a.** Representative images of CD31 stained brain sections 7 days post-RT (overview scale bar: 500 µm; zoom scale bar: 25 µm; magnification 20x). **b.** $CD31^+$ microvascular density (MVD) was shown for each condition (n_{Ctrl}= 5, n_{SDR}= 5, n_{FLASH}= 5 brains).

Data are presented as box and whiskers plots (min, max; horizontal line represents median). Groups were compared using ANOVA Tukey's post-hoc test.

FLASH RT exhibits reduced microglia/macrophages activation

Both SDR and FLASH RT decreased the ramified (surveilling [28]) Iba1$^+$ microglia/macrophage population (Fig. 4). Considering the morphology of Iba1$^+$ microglia/macrophages after radiotherapy, we could observe a more prominent rounded cell shape in treated groups (Fig. 4a), which is commonly associated to the activated phenotype [29]. Images of the tissue sections in the FLASH group indicated mixed presence of both ramified and round microglia, but this observation could not be statistically confirmed.

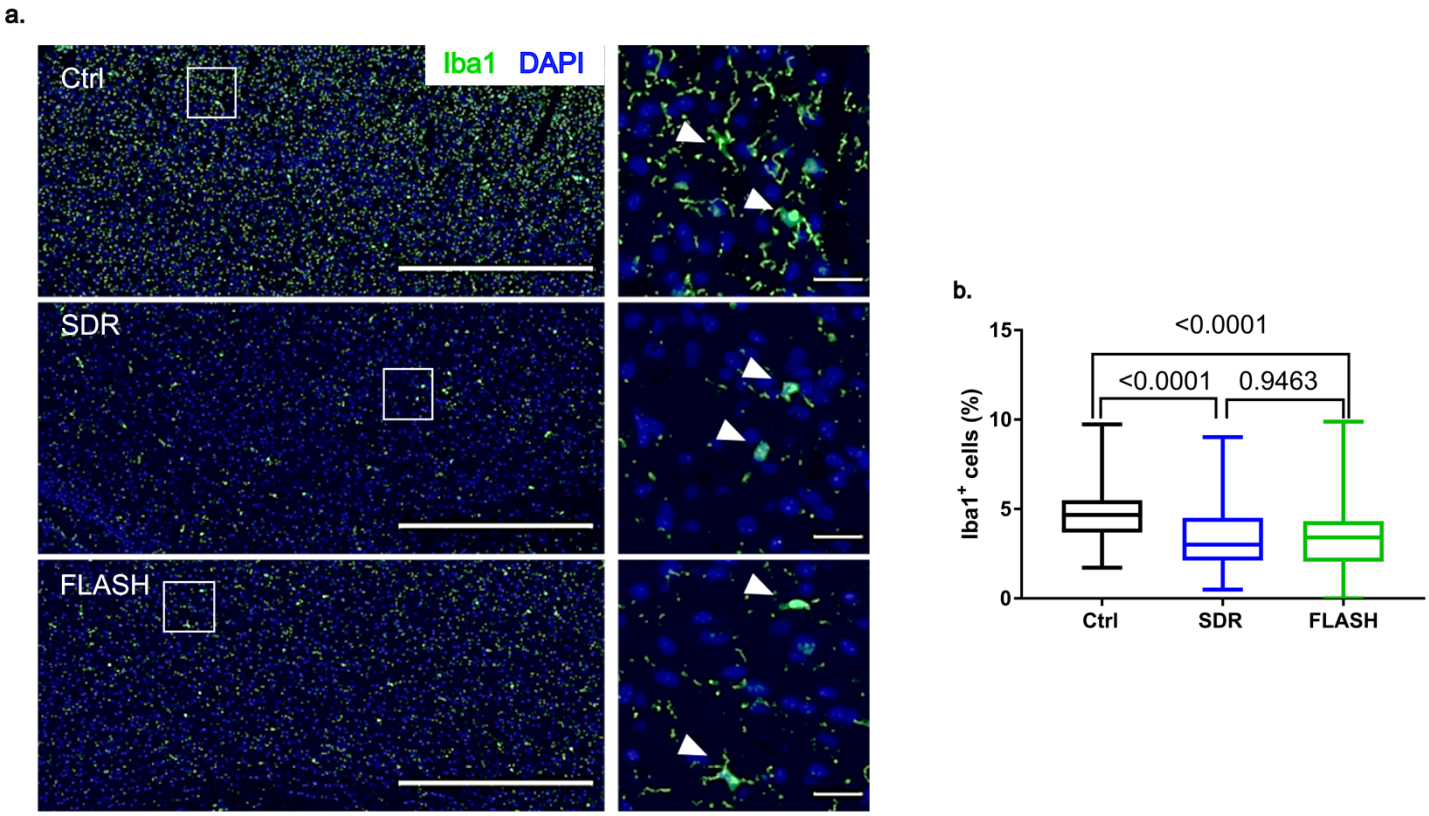

Figure 4. Radiotherapy decreases levels of ramified microglia. **a**. Representative images of Iba1$^+$ microglia 7 days post- irradiation of the mouse brain cortex (overview scale bar: 500 µm; zoom scale bar: 25 µm; magnification 20x). Arrow heads indicate ramified microglia in Ctrl group, and more rounded microglial morphology in SDR and FLASH groups. **b.** Quantification of Iba1$^+$ cells. Data are presented as box and whiskers plots (min, max; horizontal line represents median; n_{Ctrl}= 5, n_{SDR}= 5, n_{FLASH}= 5 brains). Groups were compared using ANOVA Tukey's post-hoc test.

SDR RT induced a significant increase in the cellular fraction of $CD68^+$ microglia/macrophages (p= 0.0001). FLASH RT and control samples showed a similar percentage of the $CD68^+$ population (Fig. 5b). $CD68^+$ cells were characterized by an ameboid shape (Fig. 5a), which is representative of activated, phagocytic microglia/macrophages [24]. Another hallmark of microglia/macrophages activation is an increase in iNOS expressing cell population, which could be observed after SDR RT (p= 0.0268; Fig. 5c). iNOS expression was evident in most of $CD68^+$ cells (Fig. 5a). SDR treatment led to an increase of this double-stained population when compared to the control (p= 0.0002) or FLASH irradiated tissues (p= 0.0038). Control and FLASH samples were characterized by similarly low levels of $CD68^+iNOS^+$ cells (Fig. 5d).

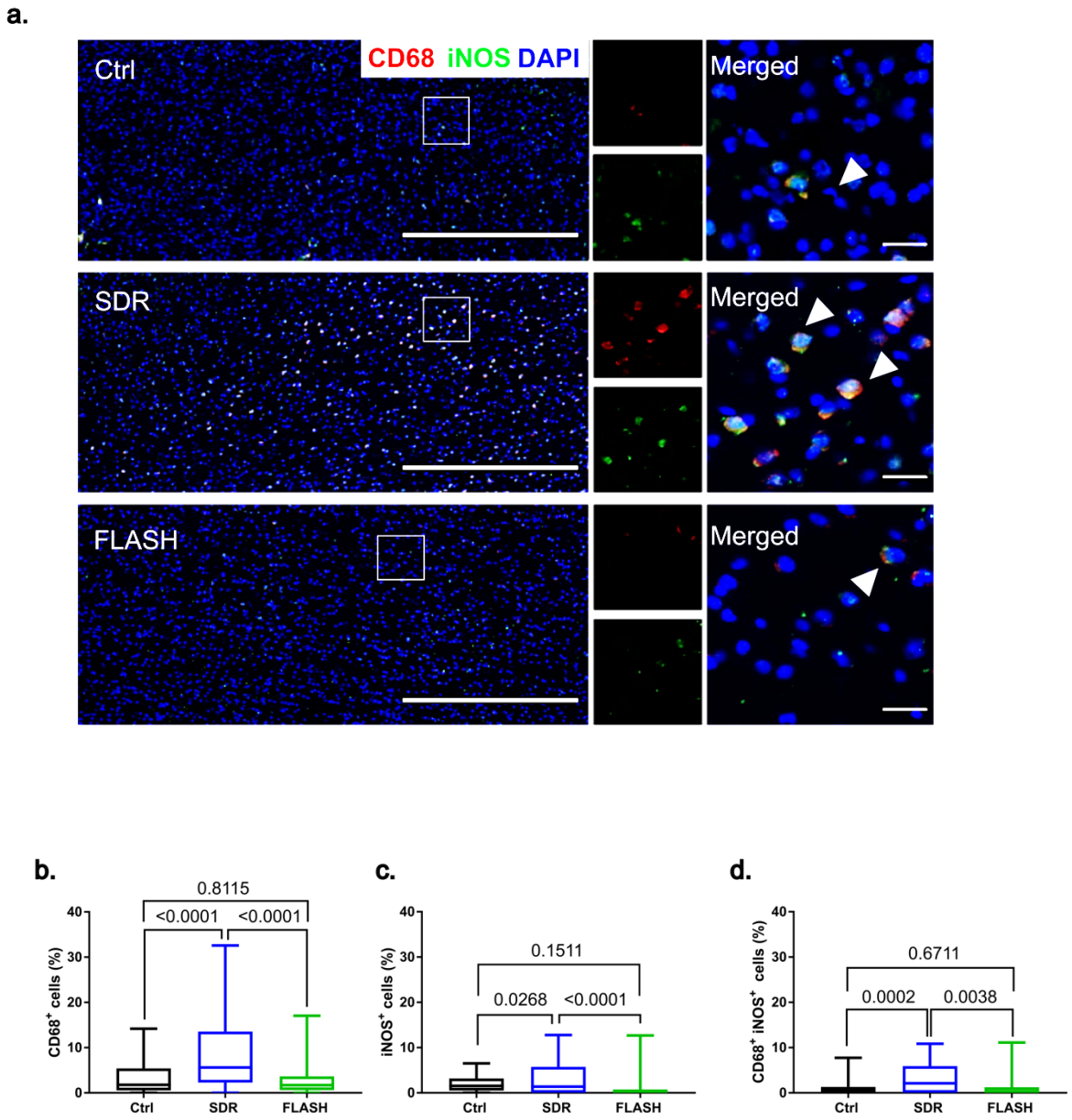

Figure 5. FLASH radiotherapy results in reduced phagocytic microglia/macrophages activation. **a**. Representative images of $CD68^+$ and $iNOS^+$microglia/macrophages of the mouse brain cortex 7 days post-irradiation (overview scale bar: 500 µm; zoom scale bar: 25 µm; magnification 20x). Arrow heads indicate

CD68 and iNOS double positive cells. Quantification of **b.** $CD68^+$, **c.** $iNOS^+$ and **d.** $CD68^+iNOS^+$ co-stained cells. Data are presented as box and whiskers plots (min, max; horizontal line represents median; n_{Ctrl}= 5, n_{SDR}= 5, n_{FLASH}= 5 brains). Groups were compared using ANOVA Tukey's post-hoc test.

Discussion

Helium ion radiotherapy may offer advantages over conventional photon and proton therapies by minimizing damage to healthy tissues and providing comparable target coverage [30]. Combining helium ion irradiation with FLASH dose rate delivery may emerge as the therapy of choice for cases requiring higher LET and exceptional normal tissue sparing.

In this study, the FLASH effect of helium ion radiotherapy was examined in preclinical settings in vivo. For this purpose, healthy mouse cortex was irradiated with 10 Gy helium ions using either ultra-high dose rate (FLASH) or standard dose rate (SDR). We compared the impact of helium FLASH radiation to SDR radiation on brain toxicity focusing on two aspects: the formation of DNA double-strand breaks (DSB) and the structural integrity of the neurovascular unit in the cerebral cortex (the microvascular endothelium and the activation of microglia/macrophages). In comparison to SDR, FLASH radiotherapy led to the reduced accumulation of the DSB DNA-damage which was visualized using DSB surrogate marker γH2AX [31]. γH2AX signal intensity, as well as γH2AX positive cell nuclei, were significantly lower in the FLASH group. The reduction of γH2AX signal was apparent both at 1 hour and 7 days post-RT. Reduced DNA damage after FLASH therapy is consistent with previous in vivo observations after proton FLASH irradiation [6, 27], in vitro using ultra-high dose rate helium beams in low oxygen condition [9] and ex-vivo using ultra-high dose rate electrons [32].

Irradiation-induced brain injury has been linked to microvascular endothelial damage, glial cell destruction, and inflammation, leading to a disruption of the neurovascular unit [33]. These adverse effects on brain tissue have been previously reported for helium irradiation [23, 34]. An increase in $CD68^+$ microglia and an upregulation of iNOS after SDR therapy in this work, aligns with existing literature that suggests irradiation-mediated microglial activation [35]. The co-expression of CD68 and iNOS is frequently associated with pro-inflammatory and phagocytic microglia/macrophages [25]. Here we demonstrate that at least a part of these side effects can be mitigated when helium ions are delivered at FLASH dose rate. SDR treatment led to an increase in activated microglia/macrophages ($CD68^+$), while significantly reducing $CD31^+$ endothelial structures. In contrast, FLASH treatment had minimal impact on the $CD68^+$ population but moderately reduced $CD31^+$ structures compared to control. This is in line with a previous study showcasing neuroprotective effects of proton FLASH beams [27] and complementary to the literature indicating electrons FLASH sparing of CNS vasculature [36] and neurocognitive function [8]. Interestingly, both SDR and FLASH RT decreased $Iba1^+$ ramified microglia (also called surveilling microglia) morphology, often associated with their physiological state [28, 37]. Even though several studies have reported a reduction in Iba1 expression following radiotherapy [38-40], the complex role of microglial activation following irradiation injury remains only partially deciphered [15]. However, transition of microglia to a pro-inflammatory state may lead to neural and endothelial tissue damage [41]. Microglia interacts with endothelial cells to maintain a stable brain environment and regulate BBB integrity [25]. Dysregulation of these interactions can lead to neurological diseases, emphasizing the importance of the microglia-endothelium

connection in brain health. Reduced microglial transition to the pro-inflammatory phenotype after FLASH irradiation, together with preservation of the $CD31^+$ microvascular endothelium, indicates benefits of FLASH helium ions in preserving brain microenvironment.

This is, to the best of our understanding, the first report providing evidence of the neuroprotective impact of FLASH helium irradiation in vivo, with an emphasis on the plasticity of microglia. This research lays the groundwork for further exploration of the FLASH effect on dynamic interaction between the brain endothelium and microglia which are crucial for neuroprotection and potential functional recovery after radiotherapy. Future studies should also examine these effects at later stages to understand the long-term benefits of FLASH radiotherapy. This will enhance our understanding of FLASH's full clinical potential.

Conclusion

This work validates the potential of FLASH raster scanning helium ions to induce FLASH sparing effect in cerebral tissue, as compared to standard dose rate in a preclinical in vivo model. Furthermore, this investigation paves the way for additional scrutiny of the ultra-high dose rate effect in particle therapy, which can be relevant in the context of advancing therapeutic strategies in radiation oncology.

References

1. Mairani, A., et al., *Roadmap: helium ion therapy.* Phys Med Biol, 2022. **67**(15).
2. Besuglow, J., et al., *The Evolution of Lateral Dose Distributions of Helium Ion Beams in Air: From Measurement and Modeling to Their Impact on Treatment Planning.* Frontiers in Physics, 2022. **9**.
3. Tessonnier, T., et al., *Proton and helium ion radiotherapy for meningioma tumors: a Monte Carlo-based treatment planning comparison.* Radiat Oncol, 2018. **13**(1): p. 2.
4. Mairani, A., et al., *Back to the Future: Helium Ion Therapy 2020.* International Journal of Radiation Oncology Biology Physics, 2020. **108**(3): p. S67-S68.
5. Velalopoulou, A., et al., *FLASH Proton Radiotherapy Spares Normal Epithelial and Mesenchymal Tissues While Preserving Sarcoma Response.* Cancer Res, 2021. **81**(18): p. 4808-4821.
6. Kim, K., et al., *FLASH Proton Radiation Therapy Mitigates Inflammatory and Fibrotic Pathways and Preserves Cardiac Function in a Preclinical Mouse Model of Radiation-Induced Heart Disease.* Int J Radiat Oncol Biol Phys, 2024.
7. Montay-Gruel, P., et al., *Long-term neurocognitive benefits of FLASH radiotherapy driven by reduced reactive oxygen species.* Proc Natl Acad Sci U S A, 2019. **116**(22): p. 10943-10951.
8. Montay-Gruel, P., et al., *Hypofractionated FLASH-RT as an Effective Treatment against Glioblastoma that Reduces Neurocognitive Side Effects in Mice.* Clin Cancer Res, 2021. **27**(3): p. 775-784.
9. Tessonnier, T., Walsh, D., Mein, S., et al., FLASH Dose Rate Helium Ion Beams: First In Vitro Investigations. Int J Radiat Oncol Biol Phys. 2021 Nov 15;111(4):1011-1022.
10. Ghannam, Y., et al., *First evidence of in vivo effect of FLASH radiotherapy with helium ions in zebrafish embryos.* Radiother Oncol, 2023. **187**: p. 109820.
11. Iadecola, C., *The Neurovascular Unit Coming of Age: A Journey through Neurovascular Coupling in Health and Disease.* Neuron, 2017. **96**(1): p. 17-42.

12. Attwell, D., et al., *Glial and neuronal control of brain blood flow.* Nature, 2010. **468**(7321): p. 232-43.
13. Lertkiatmongkol, P., et al., *Endothelial functions of platelet/endothelial cell adhesion molecule-1 (CD31).* Curr Opin Hematol, 2016. **23**(3): p. 253-9.
14. Wimmer, I., et al., *PECAM-1 Stabilizes Blood-Brain Barrier Integrity and Favors Paracellular T-Cell Diapedesis Across the Blood-Brain Barrier During Neuroinflammation.* Front Immunol, 2019. **10**: p. 711.
15. Voshart, D.C., et al., *Radiotherapy induces persistent innate immune reprogramming of microglia into a primed state.* Cell Rep, 2024. **43**(2): p. 113764.
16. Norris, G.T. and J. Kipnis, *Immune cells and CNS physiology: Microglia and beyond.* J Exp Med, 2019. **216**(1): p. 60-70.
17. Hanisch, U.K. and H. Kettenmann, *Microglia: active sensor and versatile effector cells in the normal and pathologic brain.* Nat Neurosci, 2007. **10**(11): p. 1387-94.
18. Nimmerjahn, A., F. Kirchhoff, and F. Helmchen, *Resting microglial cells are highly dynamic surveillants of brain parenchyma in vivo.* Science, 2005. **308**(5726): p. 1314-8.
19. Wendeln, A.C., et al., *Innate immune memory in the brain shapes neurological disease hallmarks.* Nature, 2018. **556**(7701): p. 332-338.
20. Voshart, D.C., et al., *Proton therapy induces a local microglial neuroimmune response.* Radiother Oncol, 2024. **193**: p. 110117.
21. Greene-Schloesser, D. and M.E. Robbins, *Radiation-induced cognitive impairment--from bench to bedside.* Neuro Oncol, 2012. **14 Suppl 4**(Suppl 4): p. iv37-44.
22. Perego, C., S. Fumagalli, and M.G. De Simoni, *Temporal pattern of expression and colocalization of microglia/macrophage phenotype markers following brain ischemic injury in mice.* J Neuroinflammation, 2011. **8**: p. 174.
23. Allen, B.D., et al., *Mitigation of helium irradiation-induced brain injury by microglia depletion.* J Neuroinflammation, 2020. **17**(1): p. 159.
24. Vilhardt, F., *Microglia: phagocyte and glia cell.* Int J Biochem Cell Biol, 2005. **37**(1): p. 17-21.
25. Gao, C., et al., *Microglia in neurodegenerative diseases: mechanism and potential therapeutic targets.* Signal Transduct Target Ther, 2023. **8**(1): p. 359.
26. Picon-Pages, P., J. Garcia-Buendia, and F.J. Munoz, *Functions and dysfunctions of nitric oxide in brain.* Biochim Biophys Acta Mol Basis Dis, 2019. **1865**(8): p. 1949-1967.
27. Dokic, I., et al., Neuroprotective Effects of Ultra-High Dose Rate FLASH Bragg Peak Proton Irradiation. Int J Radiat Oncol Biol Phys. 2022 Jul 1;113(3):614-623.
28. Tremblay, M.E., et al., *The role of microglia in the healthy brain.* J Neurosci, 2011. **31**(45): p. 16064-9.
29. Colonna, M. and O. Butovsky, *Microglia Function in the Central Nervous System During Health and Neurodegeneration.* Annu Rev Immunol, 2017. **35**: p. 441-468.
30. Wickert, R., et al., *Radiotherapy with Helium Ions Has the Potential to Improve Both Endocrine and Neurocognitive Outcome in Pediatric Patients with Ependymoma.* Cancers (Basel), 2022. **14**(23).
31. Kinner, A., et al., *Gamma-H2AX in recognition and signaling of DNA double-strand breaks in the context of chromatin.* Nucleic Acids Res, 2008. **36**(17): p. 5678-94.
32. Cooper, C.R., et al., *FLASH irradiation induces lower levels of DNA damage ex vivo, an effect modulated by oxygen tension, dose, and dose rate.* Br J Radiol, 2022. **95**(1133): p. 20211150.
33. Klos, J., et al., *Quantifying effects of radiotherapy-induced microvascular injury; review of established and emerging brain MRI techniques.* Radiother Oncol, 2019. **140**: p. 41-53.
34. Raber, J., et al., *Detrimental Effects of Helium Ion Irradiation on Cognitive Performance and Cortical Levels of MAP-2 in B6D2F1 Mice.* Int J Mol Sci, 2018. **19**(4).
35. Monje, M.L., et al., *Irradiation induces neural precursor-cell dysfunction.* Nat Med, 2002. **8**(9): p. 955-62.

36. Allen, B.D., et al., *Maintenance of Tight Junction Integrity in the Absence of Vascular Dilation in the Brain of Mice Exposed to Ultra-High-Dose-Rate FLASH Irradiation.* Radiat Res, 2020. **194**(6): p. 625-635.
37. Vidal-Itriago, A., et al., *Microglia morphophysiological diversity and its implications for the CNS.* Front Immunol, 2022. **13**: p. 997786.
38. Acharya, M.M., et al., *Elimination of microglia improves cognitive function following cranial irradiation.* Sci Rep, 2016. **6**: p. 31545.
39. Neumann, S., et al., *Cranial irradiation at early postnatal age impairs stroke-induced neural stem/progenitor cell response in the adult brain.* Sci Rep, 2020. **10**(1): p. 12369.
40. Kalm, M., et al., *Irradiation-induced loss of microglia in the young brain.* J Neuroimmunol, 2009. **206**(1-2): p. 70-5.
41. Markarian, M., et al., *Glia-Selective Deletion of Complement C1q Prevents Radiation-Induced Cognitive Deficits and Neuroinflammation.* Cancer Res, 2021. **81**(7): p. 1732-1744.